Astronomy & Astrophysics

LETTER TO THE EDITOR

Accurate abundance patterns of solar twins and analogs

Does the anomalous solar chemical composition come from planet formation?[*]

I. Ramírez[1], J. Meléndez[2], and M. Asplund[1]

[1] Max Planck Institute for Astrophysics, Postfach 1317, 85741 Garching, Germany
e-mail: ivan@mpa-garching.mpg.de
[2] Centro de Astrofísica da Universidade do Porto, Rua das Estrelas, 4150-762 Porto, Portugal

ABSTRACT

We derive the abundance of 19 elements in a sample of 64 stars with fundamental parameters very similar to solar, which minimizes the impact of systematic errors in our spectroscopic 1D-LTE differential analysis, using high-resolution ($R \simeq 60\,000$), high signal-to-noise ratio ($S/N \simeq 200$) spectra. The estimated errors in the elemental abundances relative to solar are as small as $\simeq 0.025$ dex. The abundance ratios [X/Fe] as a function of [Fe/H] agree closely with previously established patterns of Galactic thin-disk chemical evolution. Interestingly, the majority of our stars show a significant correlation between [X/Fe] and condensation temperature (T_C). In the sample of 22 stars with parameters closest to solar, we find that, on average, low T_C elements are depleted with respect to high T_C elements in the solar twins relative to the Sun by about 0.08 dex ($\simeq 20\%$). An increasing trend is observed for the abundances as a function of T_C for $900 < T_C < 1800$ K, while abundances of lower T_C elements appear to be roughly constant. We speculate that this is a signature of the planet formation that occurred around the Sun but not in the majority of solar twins. If this hypothesis is correct, stars with planetary systems like ours, although rare (frequency of $\simeq 15\%$), may be identified through a very detailed inspection of the chemical compositions of their host stars.

Key words. stars: abundances – Sun: abundances – planetary systems

1. Introduction

Standard spectroscopic abundance analyses suffer from a variety of systematic errors that are difficult to remove. Using the highest quality data, errors in stellar parameters, atomic/molecular data, the use of static/homogeneous model atmospheres, and the assumption of local thermodynamic equilibrium set an optimistic lower limit of about 0.05 dex (~10%) to the accuracy of abundance determinations (e.g., Asplund 2005). A simple way to minimize the impact of these uncertainties is to perform differential analyses of stars that are very similar to each other so that systematic errors are largely cancelled out. Naturally, attempts have been made using stars with parameters that are very similar to solar, the so-called solar twins (e.g., Meléndez et al. 2006; Meléndez & Ramírez 2007). Recent work on very high-quality spectra of a few solar twins suggests that it is even possible to reach 0.01 dex accuracy (~2%, Meléndez et al. 2009). This level of precision can be useful for revealing the fine details of abundance trends and, perhaps more importantly, to determine whether the solar chemical composition is anomalous.

The use of the Sun as a reference star is understandable. Its basic properties (effective temperature, luminosity, mass, radius, and age) are very well known, and spectra of high quality are available or can be easily acquired. Defining a good sample of solar twins is a more difficult task (Cayrel de Strobel 1996). Stars with fundamental parameters very similar to solar exist (e.g.,

Porto de Mello & da Silva 1997; Meléndez et al. 2006; Takeda et al. 2007; Meléndez & Ramírez 2007), yet when more detailed analyses of their chemical compositions or evolutionary states are made, some differences arise, such as the apparently low Li abundance of the Sun and the older age of HIP 56948, the best solar twin known to date (Meléndez & Ramírez 2007; Takeda & Tajitsu 2009). However, solar twins with Li abundances and ages similar to those of the Sun most likely exist (Pasquini et al. 2008), while the age of HIP 56948 may have been overestimated (Do Nascimento et al. 2009). In any case, although the Sun is probably not unique, it does not seem to be a very common object in the solar neighborhood (e.g., Gustafsson 2008).

Determining the detailed chemical composition of the Sun compared to other stars in the solar vicinity will help us determine how unusual our star is, and perhaps even why. Previous studies have been inconclusive because of the systematic errors described above, and because the relevant differences may be small. Here we derive precise abundances for a carefully selected sample of solar twins and analogs, for which systematic errors are minimized using differential analysis, and speculate about the nature of the abundance trends found.

2. Sample, data, and analysis

Our sample stars were selected from the *Hipparcos* catalog by applying constraints on color, based on the color-$T_{\rm eff}$ calibrations by Ramírez & Meléndez (2005), corrected by suspected zero point errors (Casagrande et al. 2009), trigonometric parallaxes, and literature values for [Fe/H] and chromospheric

---

[*] Figure 1 and Tables 1–4 are only available in electronic form at http://www.aanda.org

activity, if available. About 100 stars satisfied our selection criteria and, given our observational constraints, data for 64 of them were acquired. We also observed the asteroids Vesta and Ceres as solar reference.

Spectra were obtained with the Robert G. Tull coudé spectrograph (Tull et al. 1995) on the 2.7 m Harlan J. Smith Telescope at McDonald Observatory in April, October, and November of 2007. The spectral resolution is $R = \lambda/d\lambda \simeq 60\,000$ and the wavelength coverage 3800–9125 Å, with gaps between echelle orders of 10–100 Å for wavelengths longer than 6100 Å. Typically two exposures of 20–30 min each were obtained per star with a resulting signal-to-noise ratio (S/N) of at least 150 (median $S/N \simeq 200$). Equivalent widths (EWs) were measured in the spectra (reduced, wavelength calibrated, and normalized using standard techniques) employing four different methods. From comparisons of EW determinations in different spectra for the same star, we estimate that the individual errors in EW are between 2 and 10%, depending on S/N and EW.

We compiled a line list of features that are mostly unblended in the spectra of solar-type stars. This line list includes 25 Fe I lines covering a wide range of excitation potential (EP = 0 to 5 eV) and line strength ($EW = 10$ to 120 m Å), as well as five Fe II features, which facilitate precise determination of stellar parameters (see below). The majority of the other elements analyzed in this work have between three and eleven available features (C, O, Al, Si, S, Ca, Sc, Ti, V, Cr, Mn, Ni, Ba), while the rest have less than three (Na, Cu, Zn, Y, Zr).

Effective temperatures, surface gravities, and microturbulent velocities were determined with the standard spectroscopic technique of excitation/ionization balance of iron lines. Recently computed Kurucz model atmospheres (Castelli & Kurucz 2003) and the spectrum synthesis program MOOG (Sneden 1973) were used to determine the abundance of iron ([Fe/H])[1] from the Fe I and Fe II lines. For a given set of parameters, we measured the [Fe/H] vs. excitation potential and [Fe/H] vs. reduced equivalent width ($REW = \log EW/\lambda$) slopes for the Fe I lines, as well as the difference in the mean [Fe/H] obtained from the Fe I and Fe II lines separately. The stellar parameters were then modified iteratively so that the slopes and the Fe I minus Fe II difference approached zero. This procedure was done without subjective human interaction and led to unique solutions, even though our Fe I linelist showed a mild correlation between EP and REW. The 1-σ uncertainty of the slopes and Fe I minus Fe II difference were used to determine the observational errors (average values given here): $\sigma(T_{\rm eff}) = 50$ K, $\sigma(\log g) = 0.07$ dex, and $\sigma([{\rm Fe/H}]) = 0.024$ dex. Hereafter, the 22 stars with $T_{\rm eff}$ within 100 K, $\log g$ within 0.1 dex and [Fe/H] within 0.1 dex of the solar values are referred to as solar twins.

The abundances of the 18 other elements were calculated with MOOG, using the appropriate Kurucz model atmosphere and the curve-of-growth technique. The solar abundances, derived from our asteroid spectra, were used to determine relative abundances of each star on a line-by-line basis. We did not require extremely accurate absolute solar abundances for our analysis, which is entirely differential. Since almost all lines analyzed by us are well within the linear part of the curve of growth (the exceptions being a few strong Fe I and Ba II lines), the uncertainties in our derived solar abundances and/or adopted transition probabilities are irrelevant. The average and standard deviation of the line-by-line relative abundances were adopted as the final abundance, [X/H], and error. On average, the [X/H] values

have line-by-line uncertainties of ≃0.025 dex. Errors in the parameters affect [X/H] and [Fe/H] similarly so that [X/Fe] abundance ratios are relatively insensitive to those uncertainties. The average error in [X/Fe] is ≃0.03 dex, which is dominated by the line-by-line scatter of the X and Fe elemental abundances. To improve the accuracy, non-LTE corrections were applied to the derived oxygen abundances using the results by Ramírez et al. (2007), while hyperfine structure was taken into account in the synthesis of Mn and V lines (Prochaska & McWilliam 2000; Johnson et al. 2006).

Our derived stellar parameters and abundances are available online (Tables 1 to 4).

3. Abundance trends among solar twin stars

In Fig. 1 (available online), we show the abundance ratios [X/Fe] determined in this work as a function of [Fe/H]. When compared to the abundance trends for Galactic thin-disk stars published elsewhere (e.g., Bensby et al. 2005; Reddy et al. 2006; Takeda 2007; Neves et al. 2009), we notice that the slopes and relative scatter (between different elements) are compatible with our results (all but the two most metal-poor stars in our sample have thin-disk kinematics). However, there is no general agreement about the zero points of the abundance ratios, which is a consequence of systematic errors that affect the various techniques used by other authors differently. Since those errors have been minimized in our differential work, the zero points of the abundance scales reported here should be reliable.

The decreasing [X/Fe] vs. [Fe/H] trends for C, O, S, Ca, Sc, and Ti are consistent with currently accepted interpretations of thin-disk chemical evolution (e.g., McWilliam 1997). Al, Si, and Zn also show this trend but the slope is too shallow to produce a noticeable effect in our data, given the short [Fe/H] range. This is attributed to the increasing importance of the type Ia supernovae (SNe) contribution to the interstellar medium (ISM) composition compared to type II SNe. The very steep increase in [Mn/Fe] with [Fe/H] can be understood as metallicity-dependent yields from SNe II. The nearly constant Na, V, Cr, Ni, and Cu abundance ratios stem from these elements and Fe roughly having the same nucleosynthetic origins. The abundance ratios of the s-process elements Y, Zr, and in particular Ba, which are thought to be produced mainly in AGB stars, are strongly dependent on stellar age (e.g., Edvardsson et al. 1993; Bensby et al. 2007); therefore, the large scatter seen is likely related to the age span of our sample. Also, non-negligible non-LTE effects are predicted for Ba (≃ 0.1 dex, Mashonkina et al. 1999; Mashonkina & Gehren 2000), but they have not been corrected here.

Next, we examined the relation between [X/Fe] and condensation temperature (T_C; calculated for a solar-system composition gas by Lodders 2003). Most of our sample stars show a significant correlation, although individually the scatter is relatively large (Fig. 2). Thus, we averaged the [X/Fe] values for our 22 solar twins and compared them to T_C. As seen in Fig. 3, refractory elements ($T_C > 900$ K) are overabundant with respect to the volatiles ($T_C < 900$ K) in the solar twins compared to the Sun by as much as 20 % (≃0.08 dex). A linear fit to the $T_C > 900$ K elements, weighted by the star-to-star scatter, shows that the abundance vs. T_C correlation of refractory elements is significant at the 3σ level. The elements that depart the most from this trend are Al ($T_C = 1653$ K) and Ba ($T_C = 1455$ K). For Ba, a combination of age-related and strong non-LTE effects could be responsible for the large star-by-star scatter seen in Fig. 1 (e.g., Bensby et al. 2007; Mashonkina & Gehren 2000).
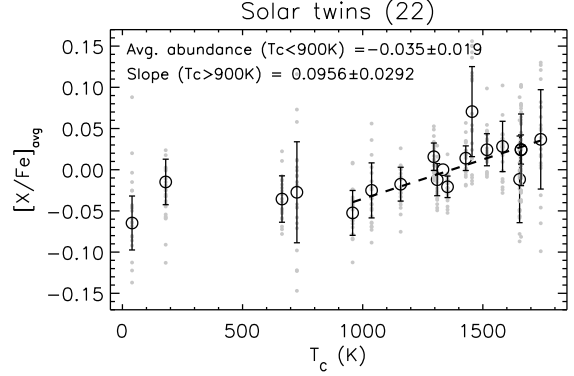
---

[1] We adopt: $A_{\rm X} = \log n_{\rm X}/n_{\rm H}+12$, where $n_{\rm X}$ is the number density of the element X; [X/H] = $A_{\rm X} - A_{\rm X}^{\odot}$; and [X/Fe] = [X/H] − [Fe/H].
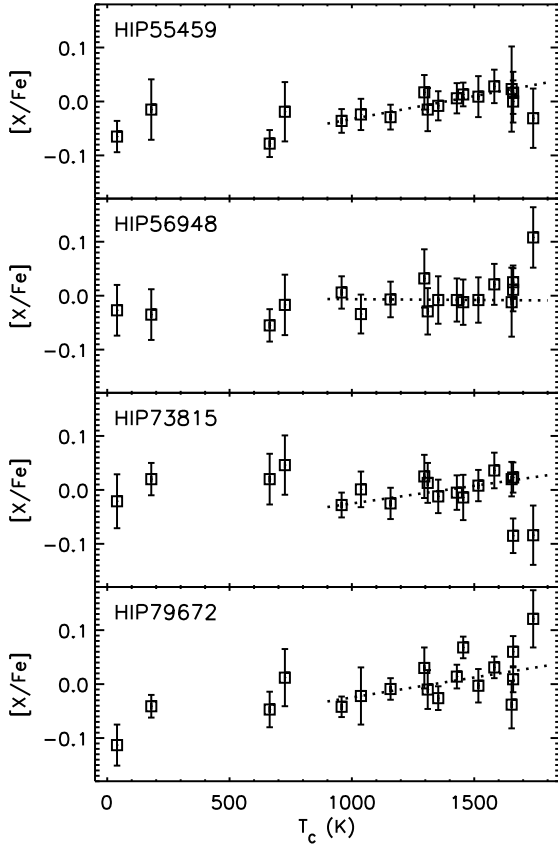
Fig. 2. Abundance ratios as a function of condensation temperature (T_C) for four of our solar twins. The dotted line is a linear fit to the abundance ratios of refractory elements ($T_C > 900$ K).

Fig. 3. Average abundance ratios of 22 solar twin stars as a function of condensation temperature (T_C). Gray solid circles represent individual abundances, while open circles with error bars correspond to the weighted average and standard deviation of all stars for each element. The open circle without error bar corresponds to iron. The dashed line is a linear fit to the abundance ratios of refractory elements.
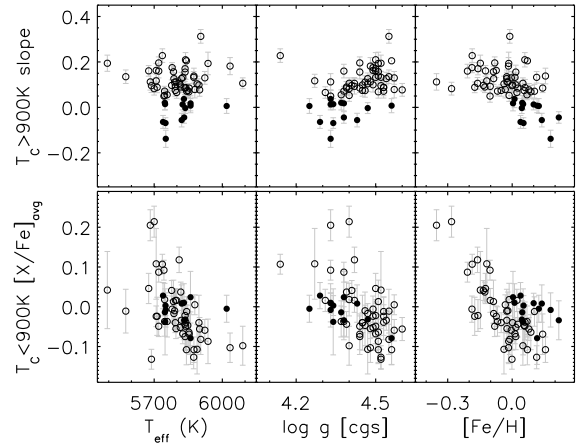
Fig. 4. *Top panel*: abundance vs. T_C slope for $T_C > 900$ K as a function of stellar parameters. *Bottom panel*: average abundance of $T_C < 900$ K elements as a function of stellar parameters. The filled circles are stars that have T_C slopes less than their 1-σ error, including stars with negative slope. Units of T_C slope are 10^{-3} dex K^{-1}.

Following the referee's suggestion, we also examined the relation between [X/Fe] and the first ionization potential (FIP). While at first sight a correlation is apparent, its significance is less than for the T_C trend (1.5σ for the $T_C > 900$ K elements). We note, in particular, that Na, an element that clearly defines the T_C trend, stands out as an obvious outlier on the FIP correlation. Moreover, if the abundances are plotted against the ionization potential of the species that correspond to the spectral lines used in our work (Y, Zr, and Ba abundances were derived from their singly ionized lines), the (already weak) correlation disappears.

To further examine the correlation with T_C, we show the relation between the abundance ratio vs. T_C slope for the refractory elements ($T_C > 900$ K) and stellar parameters in Fig. 4. We also show there the relation between the average abundance ratio of volatiles ($T_C < 900$ K) and stellar parameters. The $T_C > 900$ K slopes and $T_C < 900$ K average abundances plotted in Fig. 4 are listed in Table 1, available online. The trend seen for the average abundance of volatiles vs. [Fe/H] relation comes from chemical evolution effects, given that the abundance ratios of C and O increase with lower [Fe/H] (Fig. 1). The $T_C > 900$ K slope is correlated with the stellar surface gravity ($\log g$) and [Fe/H]. Furthermore, at super-solar metallicities, there seem to be two distinct groups of stars, one showing positive slope and underabundance of volatiles and the other one having negative slope and roughly solar abundance of volatiles. A Kolmogorov-Smirnov test shows that the likelihood that the distribution of slopes at [Fe/H] > 0 corresponds to a single Gaussian centered around zero is about 2.7 times less than that of two Gaussians centered on -0.05 and 0.09×10^{-3} dex K^{-1}, respectively

(assuming a width of 0.03×10^{-3} dex K^{-1}, which is the average observed value of our 22 solar twins).

Given the very limited [Fe/H] range (=0.0 ± 0.1 dex), Galactic chemical evolution effects are unimportant for our solar twins sample, and so the trend with T_C shown in Fig. 3 is most likely related to other processes. Similar abundance trends with T_C have been found for the ISM (e.g., Savage & Sembach 1996) and for certain types of objects such as post-AGB, RV Tauri, and λ Bootis stars (e.g., Venn & Lambert 1990; Giridhar et al. 2005), albeit with much larger amplitudes. In the case of λ Bootis stars, the T_C trend is attributed to the accretion of volatile rich gas with refractories depleted into grains in a fashion qualitatively consistent with ISM depletion patterns. In the atmospheres of the majority of our solar twins, elements that are more likely to form dust grains are more overabundant compared to the Sun. If the Sun and its twins formed similarly (in particular from gas with very similar initial chemical composition), where did the refractory elements go in the solar case?

4. Planetary signatures in the abundance trends?

Meléndez et al. (2009), who were the first to detect the T_C abundance trends that we confirm in this paper, suggest that the

I. Ramírez et al.: Abundance patterns of solar twins

solar chemical composition has been affected by the formation of planets. Inner solar system objects are enriched in refractory elements relative to volatiles (e.g., Palme 2000), mirroring the trend seen in Fig. 3. Relative abundances in meteorites are roughly constant up to $T_C \simeq 1000\,K$ but increase steeply with T_C for $T_C \gtrsim 1000\,K$ (Alexander et al. 2001, their Fig. 2). In the solar twins compared to the Sun, the overabundance of refractory elements relative to volatiles is of about 20% (or 0.08 dex). An order of magnitude calculation shows that such a difference would roughly disappear if the total mass of refractory elements in the terrestrial planets of the solar system today were to be added to the solar convective zone (Meléndez et al. 2009). If the majority of solar twins did not form planets, their original chemical compositions should not have been altered, with no deficiency of refractories, as observed. The near constancy of the abundance of volatiles ($T_C \lesssim 1000\,K$) and the fact that they do not condense at the high temperatures present in the inner proto-solar system suggest that the Sun and its twins have retained those elements. The abundance differences for the volatiles would dissapear on average had we chosen one of those elements as the reference element rather than the refractory element Fe.

The behavior of the $T_C > 900\,K$ slope with metallicity is particularly interesting (Fig. 4). At solar and sub solar metallicity, few stars have near zero slope (within their 1-σ error). At super-solar metallicities, however, there seem to be two groups of stars: one showing positive T_C slope and the other one negative. Following our line of reasoning, a negative slope implies that an even greater fraction of refractory elements have been extracted from the star-forming cloud to make up dust grains, also suggesting planet formation. Since the frequency of planetary systems increases with [Fe/H] (e.g., Udry & Santos 2007), it is tempting to conclude that this bimodal distribution is separating super-solar metallicity stars with and without terrestrial planets. Thus, while for [Fe/H] $\lesssim 0.1$ the fraction of stars showing the proposed "planet signature" in their chemical composition is $\simeq 15\%$, for [Fe/H] > 0.1 the number is $\simeq 50\%$ or more. The low number of stars analyzed at high [Fe/H] prevent us from determining this number more accurately.

Certainly, our interpretation of the T_C trend may be questioned. For example, that the currently accepted values for the lifetimes of observed disks around pre-main-sequence stars are too short (~ 3 to $10\,Myr$; e.g., Meyer 2009), compared to the time it took the solar convective zone to reach its present size ($\sim 30\,Myr$; e.g., D'Antona & Mazzitelli 1994), suggests that the planet signature could not have been imprinted into the photospheric composition. However, recent realistic star formation calculations suggest that the structure of the early Sun was similar to that of the present one, and never fully convective (Wuchterl & Klessen 2001; Wuchterl & Tscharnuter 2003), which would solve the time-scale problem (Nordlund 2009).

Independently of the interpretation, the observational result that the solar chemical composition is anomalous when compared to solar-type stars is very robust. We have minimized systematic errors by using differential analysis and reduced observational scatter by averaging the results over many stars that are similar to each other.

Previous studies (e.g., Smith et al. 2001; Takeda et al. 2001; Santos et al. 2004; Ecuvillon et al. 2006; Gonzalez & Laws 2007) have been cautious about reaching strong conclusions based on abundance trends with T_C because of the still relatively large systematic errors associated with their analyses in comparison with the small size of the effect. To detect this trend, a precision of $\simeq 0.03$ dex or better is required. In fact, as stated above, the T_C trend shown in Fig. 3 was first detected by Meléndez et al. (2009), who were able to achieve a precision of 0.01 dex in their derived abundance ratios using spectra of higher quality for eleven southern hemisphere solar twins.

Detecting planets around other stars is one of the major challenges of contemporary astrophysics. Current technology allows us to find giant planets in close-in orbits with relative ease, so remarkable progress is being made in our understanding of exoplanets (e.g., Udry & Santos 2007). Terrestrial planets and solar system analogs, however, remain elusive. The possibility of identifying them using detailed chemical composition analyses is therefore very promising. There is no reason to restrict this experiment to solar twins, because any group of stars twins of each other can be used to measure very precise relative abundances. We are currently working on the homogeneous (i.e., same telescope/instrument/observing conditions) acquisition and analysis of very high-quality spectra ($R \simeq 100,000$; $S/N \gtrsim 400$) of stars with and without detected planets to continue this investigation.

References

Alexander, C. M. O., Boss, A. P., & Carlson, R. W. 2001, Science, 293, 64
Asplund, M. 2005, ARA&A, 43, 481
Bensby, T., Feltzing, S., Lundström, I., & Ilyin, I. 2005, A&A, 433, 185
Bensby, T., Zenn, A. R., Oey, M. S., & Feltzing, S. 2007, ApJ, 663, L13
Casagrande, L., Ramírez, I., Meléndez, J., Asplund, M., & Bessell, M. 2009, A&A, submitted
Castelli, F., & Kurucz, R. L. 2003, in Modelling of Stellar Atmospheres, ed. N. Piskunov, W. W. Weiss, & D. F. Gray, IAU Symp., 210, 20P
Cayrel de Strobel, G. 1996, A&A Rev., 7, 243
D'Antona, F., & Mazzitelli, I. 1994, ApJS, 90, 467
Do Nascimento, Jr., J. D., Castro, M., Meléndez, J., et al. 2009, A&A, 501, 687
Ecuvillon, A., Israelian, G., Santos, N. C., Mayor, M., & Gilli, G. 2006, A&A, 449, 809
Edvardsson, B., Andersen, J., Gustafsson, B., et al. 1993, A&A, 275, 101
Giridhar, S., Lambert, D. L., Reddy, B. E., Gonzalez, G., & Yong, D. 2005, ApJ, 627, 432
Gonzalez, G., & Laws, C. 2007, MNRAS, 378, 1141
Gustafsson, B. 2008, Phys. Scr. T, 130, 014036
Johnson, J. A., Ivans, I. I., & Stetson, P. B. 2006, ApJ, 640, 801
Lodders, K. 2003, ApJ, 591, 1220
Mashonkina, L., & Gehren, T. 2000, A&A, 364, 249
Mashonkina, L., Gehren, T., & Bikmaev, I. 1999, A&A, 343, 519
McWilliam, A. 1997, ARA&A, 35, 503
Meléndez, J., & Ramírez, I. 2007, ApJ, 669, L89
Meléndez, J., Dodds-Eden, K., & Robles, J. A. 2006, ApJ, 641, L133
Meléndez, J., Asplund, M., Gustafsson, B., & Yong, D. 2009, ApJ, 704, L66
Meyer, M. R. 2009, in IAU Symp. 258, ed. E. E. Mamajek, D. R. Soderblom, & R. F. G. Wyse, 111
Neves, V., Santos, N. C., Sousa, S. G., Correia, A. C. M., & Israelian, G. 2009, A&A, 497, 563
Nordlund, A. 2009, ApJ, submitted [arXiv:0908.3479]
Palme, H. 2000, Space Sci. Rev., 92, 237
Pasquini, L., Biazzo, K., Bonifacio, P., Randich, S., & Bedin, L. R. 2008, A&A, 489, 677
Porto de Mello, G. F., & da Silva, L. 1997, ApJ, 482, L89
Prochaska, J. X., & McWilliam, A. 2000, ApJ, 537, L57
Ramírez, I., & Meléndez, J. 2005, ApJ, 626, 465
Ramírez, I., Allende Prieto, C., & Lambert, D. L. 2007, A&A, 465, 271
Reddy, B. E., Lambert, D. L., & Allende Prieto, C. 2006, MNRAS, 367, 1329
Santos, N. C., Israelian, G., & Mayor, M. 2004, A&A, 415, 1153
Savage, B. D., & Sembach, K. R. 1996, ARA&A, 34, 279
Smith, V. V., Cunha, K., & Lazzaro, D. 2001, AJ, 121, 3207
Sneden, C. A. 1973, Ph.D. Thesis, The University of Texas at Austin
Takeda, Y. 2007, PASJ, 59, 335
Takeda, Y., & Tajitsu, A. 2009, PASJ, 61, 471
Takeda, Y., Sato, B., Kambe, E., et al. 2001, PASJ, 53, 1211
Takeda, Y., Kawanomoto, S., Honda, S., Ando, H., & Sakurai, T. 2007, A&A, 468, 663
Tull, R. G., MacQueen, P. J., Sneden, C., & Lambert, D. L. 1995, PASP, 107, 251
Udry, S., & Santos, N. C. 2007, ARA&A, 45, 397
Venn, K. A., & Lambert, D. L. 1990, ApJ, 363, 234
Wuchterl, G., & Klessen, R. S. 2001, ApJ, 560, L185
Wuchterl, G., & Tscharnuter, W. M. 2003, A&A, 398, 1081

Table 1. Derived stellar parameters, average abundance ratios [X/Fe] of volatile elements ($T_C < 900$ K), and slope of the [X/Fe] vs. T_C relation for refractory elements ($T_C > 900$ K). Errors in [Fe/H] correspond to the 1-σ scatter of the line-by-line abundances.

HIP	$T_{\rm eff}$ (K)	$\log g$ [cgs]	[Fe/H]			$T_C < 900$ K avg. [X/Fe]			$T_C > 900$ K T_C slope		
348	5777	4.41	−0.132	±	0.024	0.041	±	0.025	0.097	±	0.024
996	5860	4.38	−0.001	±	0.022	0.024	±	0.065	0.018	±	0.033
1499	5751	4.33	0.180	±	0.043	−0.008	±	0.043	−0.138	±	0.038
2131	5720	4.38	−0.209	±	0.026	0.087	±	0.025	0.160	±	0.030
2894	5820	4.54	−0.023	±	0.025	−0.034	±	0.025	0.127	±	0.028
4909	5836	4.44	0.018	±	0.024	−0.075	±	0.033	0.155	±	0.030
5134	5779	4.49	−0.187	±	0.023	−0.006	±	0.033	0.175	±	0.022
6407	5787	4.47	−0.084	±	0.011	−0.017	±	0.025	0.127	±	0.025
7245	5843	4.53	0.105	±	0.023	−0.012	±	0.037	0.071	±	0.030
8507	5720	4.44	−0.079	±	0.026	−0.049	±	0.026	0.196	±	0.026
8841	5676	4.50	−0.127	±	0.021	0.046	±	0.038	0.161	±	0.024
9349	5826	4.50	0.010	±	0.019	−0.068	±	0.025	0.132	±	0.020
10710	5817	4.39	−0.130	±	0.022	0.037	±	0.025	0.090	±	0.024
11728	5747	4.37	0.049	±	0.022	−0.014	±	0.029	0.020	±	0.032
11915	5793	4.45	−0.052	±	0.021	−0.040	±	0.025	0.075	±	0.025
14614	5794	4.42	−0.103	±	0.022	0.016	±	0.030	0.092	±	0.034
14632	6019	4.25	0.124	±	0.024	−0.005	±	0.034	0.006	±	0.033
18261	5897	4.45	0.001	±	0.017	−0.040	±	0.069	0.099	±	0.027
22528	5683	4.33	−0.351	±	0.035	0.205	±	0.039	0.112	±	0.036
23835	5736	4.14	−0.183	±	0.020	0.107	±	0.025	0.228	±	0.030
25670	5757	4.37	0.066	±	0.018	−0.037	±	0.039	0.055	±	0.022
28336	5713	4.53	−0.175	±	0.027	−0.024	±	0.048	0.088	±	0.024
38072	5839	4.53	0.059	±	0.037	−0.039	±	0.044	0.087	±	0.036
38228	5688	4.52	−0.003	±	0.026	−0.132	±	0.025	0.096	±	0.030
42438	5889	4.47	−0.036	±	0.029	−0.107	±	0.062	0.104	±	0.034
44324	5937	4.51	−0.014	±	0.021	−0.087	±	0.056	0.193	±	0.050
46066	5709	4.49	−0.073	±	0.039	−0.024	±	0.026	0.163	±	0.031
49572	5831	4.33	0.008	±	0.021	0.010	±	0.048	0.037	±	0.038
49756	5900	4.60	0.081	±	0.037	−0.056	±	0.029	0.077	±	0.028
52040	5785	4.51	−0.090	±	0.021	0.013	±	0.054	0.157	±	0.024
52137	5842	4.56	0.069	±	0.026	−0.108	±	0.038	0.205	±	0.025
55459	5835	4.39	0.030	±	0.022	−0.044	±	0.032	0.085	±	0.029
56948	5837	4.47	0.044	±	0.027	−0.032	±	0.025	−0.003	±	0.024
56997	5575	4.55	−0.026	±	0.030	−0.011	±	0.055	0.135	±	0.030
60314	5874	4.52	0.115	±	0.033	−0.127	±	0.029	0.132	±	0.025
62175	5854	4.44	0.144	±	0.021	−0.069	±	0.051	0.085	±	0.020
64150	5748	4.34	0.050	±	0.020	−0.038	±	0.083	0.014	±	0.025
64497	5860	4.56	0.117	±	0.037	−0.079	±	0.066	0.007	±	0.031
64794	5743	4.33	−0.105	±	0.027	0.092	±	0.025	0.050	±	0.027
72659	5494	4.52	−0.149	±	0.039	0.042	±	0.097	0.194	±	0.036
73815	5799	4.31	0.021	±	0.022	0.016	±	0.028	0.066	±	0.026
74341	5853	4.51	0.084	±	0.026	−0.064	±	0.044	0.069	±	0.028
77466	5700	4.40	−0.280	±	0.028	0.214	±	0.039	0.082	±	0.028
78028	5879	4.57	−0.035	±	0.041	0.005	±	0.025	0.079	±	0.037
78680	5923	4.57	−0.004	±	0.027	−0.059	±	0.027	0.130	±	0.028
79186	5709	4.27	−0.119	±	0.024	0.108	±	0.089	0.117	±	0.029
79672	5848	4.46	0.055	±	0.019	−0.047	±	0.051	0.074	±	0.029
81512	5790	4.46	−0.019	±	0.025	−0.010	±	0.047	0.111	±	0.028
83601	6090	4.40	0.051	±	0.031	−0.098	±	0.049	0.106	±	0.024
88194	5746	4.38	−0.067	±	0.015	−0.037	±	0.037	0.071	±	0.021
88427	5810	4.42	−0.160	±	0.025	0.118	±	0.032	0.106	±	0.026
89443	5796	4.48	−0.026	±	0.038	−0.055	±	0.025	0.113	±	0.018
96895	5825	4.33	0.096	±	0.026	0.009	±	0.025	0.013	±	0.024
96901	5750	4.34	0.052	±	0.021	0.003	±	0.025	−0.069	±	0.023
100963	5815	4.49	0.018	±	0.019	−0.052	±	0.025	0.099	±	0.032
102152	5746	4.40	−0.013	±	0.031	0.018	±	0.041	0.052	±	0.026
104504	5836	4.50	−0.154	±	0.022	−0.022	±	0.040	0.170	±	0.027
107350	6034	4.48	−0.016	±	0.024	−0.103	±	0.037	0.182	±	0.038
108708	5875	4.51	0.152	±	0.024	−0.108	±	0.032	0.138	±	0.035
108996	5838	4.50	0.056	±	0.027	−0.049	±	0.061	0.210	±	0.032
109931	5739	4.29	0.037	±	0.026	0.028	±	0.033	−0.064	±	0.029
113357	5832	4.38	0.215	±	0.023	−0.034	±	0.049	−0.044	±	0.025
115604	5821	4.43	0.137	±	0.019	0.008	±	0.047	−0.056	±	0.030
118159	5905	4.55	−0.010	±	0.022	−0.082	±	0.038	0.313	±	0.030

Table 2. Abundance ratios [X/Fe] for C, O, Na, Al, Si, and S. Errors correspond to the 1-σ scatter of the line-by-line abundances. A conservative value of 0.050 for the error was assumed when only one line was available.

| HIP	C	O	Na	Al	Si	S
348	0.057 ± 0.037	0.050 ± 0.045	−0.039 ± 0.021	0.032 ± 0.024	−0.005 ± 0.042	0.010 ± 0.027
996	0.020 ± 0.031	−0.011 ± 0.012	0.008 ± 0.025	0.060 ± 0.022	0.029 ± 0.030	−0.030 ± 0.026
1499	−0.012 ± 0.030	−0.068 ± 0.036	0.118 ± 0.025	0.066 ± 0.043	0.015 ± 0.035	0.019 ± 0.026
2131	0.102 ± 0.030	0.094 ± 0.032	−0.060 ± 0.025	0.058 ± 0.029	0.020 ± 0.034	0.056 ± 0.070
2894	−0.044 ± 0.038	−0.057 ± 0.035	−0.078 ± 0.016	−0.059 ± 0.042	−0.042 ± 0.026	−0.026 ± 0.025
4909	−0.122 ± 0.013	−0.045 ± 0.035	−0.113 ± 0.021	−0.087 ± 0.035	−0.037 ± 0.037	−0.069 ± 0.052
5134	−0.042 ± 0.050	0.022 ± 0.038	−0.089 ± 0.012	−0.049 ± 0.026	−0.015 ± 0.040	0.022 ± 0.050
6407	−0.043 ± 0.024	−0.001 ± 0.031	−0.045 ± 0.014	−0.008 ± 0.027	0.004 ± 0.031	−0.008 ± 0.032
7245	−0.044 ± 0.013	−0.042 ± 0.043	0.005 ± 0.025	−0.034 ± 0.029	−0.026 ± 0.049	0.013 ± 0.021
8507	−0.082 ± 0.050	−0.019 ± 0.059	−0.084 ± 0.016	−0.007 ± 0.034	0.004 ± 0.079	−0.048 ± 0.053
8841	−0.000 ± 0.025	0.032 ± 0.081	−0.086 ± 0.025	−0.004 ± 0.032	−0.037 ± 0.043	0.082 ± 0.028
9349	−0.086 ± 0.025	−0.091 ± 0.118	−0.061 ± 0.011	−0.078 ± 0.015	−0.046 ± 0.046	−0.051 ± 0.061
10710	0.051 ± 0.024	0.041 ± 0.030	−0.041 ± 0.025	−0.034 ± 0.025	−0.009 ± 0.029	0.049 ± 0.063
11728	−0.047 ± 0.017	−0.030 ± 0.025	−0.024 ± 0.025	0.008 ± 0.028	−0.002 ± 0.038	0.011 ± 0.025
11915	−0.046 ± 0.012	−0.032 ± 0.061	−0.062 ± 0.018	−0.057 ± 0.015	−0.022 ± 0.031	−0.013 ± 0.064
14614	0.007 ± 0.046	−0.012 ± 0.046	−0.047 ± 0.029	0.014 ± 0.059	−0.006 ± 0.044	0.011 ± 0.025
14632	−0.003 ± 0.041	−0.034 ± 0.031	0.042 ± 0.025	0.003 ± 0.038	−0.010 ± 0.044	−0.026 ± 0.078
18261	−0.098 ± 0.048	−0.040 ± 0.036	−0.089 ± 0.025	−0.066 ± 0.013	−0.024 ± 0.025	−0.079 ± 0.086
22528	0.253 ± 0.160	0.192 ± 0.052	−0.037 ± 0.025	0.162 ± 0.041	0.063 ± 0.036	0.160 ± 0.010
23835	0.111 ± 0.052	0.139 ± 0.038	−0.017 ± 0.025	0.132 ± 0.021	0.072 ± 0.029	0.090 ± 0.011
25670	−0.092 ± 0.025	−0.038 ± 0.036	−0.041 ± 0.016	−0.002 ± 0.053	−0.012 ± 0.045	−0.012 ± 0.011
28336	−0.021 ± 0.025	−0.007 ± 0.050	−0.051 ± 0.021	−0.055 ± 0.024	−0.024 ± 0.045	0.023 ± 0.050
38072	−0.044 ± 0.035	0.001 ± 0.080	−0.038 ± 0.025	−0.001 ± 0.046	−0.001 ± 0.036	−0.013 ± 0.025
38228	−0.137 ± 0.050	−0.113 ± 0.050	−0.065 ± 0.025	−0.023 ± 0.020	−0.009 ± 0.061	
42438	−0.035 ± 0.025	−0.077 ± 0.085	−0.081 ± 0.025	−0.083 ± 0.037	−0.034 ± 0.047	−0.150 ± 0.108
44324	−0.098 ± 0.020	−0.136 ± 0.017		−0.156 ± 0.076	−0.119 ± 0.064	
46066	−0.015 ± 0.040	−0.025 ± 0.035	−0.059 ± 0.025	−0.049 ± 0.071	−0.030 ± 0.027	−0.058 ± 0.104
49572	0.029 ± 0.018	−0.048 ± 0.025	0.020 ± 0.025	0.040 ± 0.034	0.008 ± 0.048	−0.006 ± 0.020
49756	−0.020 ± 0.033	−0.066 ± 0.036	−0.029 ± 0.025	−0.037 ± 0.045	−0.031 ± 0.029	−0.051 ± 0.011
52040	0.088 ± 0.099	0.003 ± 0.043	−0.079 ± 0.012	−0.056 ± 0.052	−0.024 ± 0.039	−0.039 ± 0.050
52137	−0.157 ± 0.024	−0.065 ± 0.024	−0.086 ± 0.020	−0.064 ± 0.025	−0.023 ± 0.044	−0.106 ± 0.046
55459	−0.065 ± 0.019	−0.015 ± 0.052	−0.036 ± 0.025	0.023 ± 0.075	−0.015 ± 0.033	−0.078 ± 0.013
56948	−0.025 ± 0.039	−0.033 ± 0.039	0.008 ± 0.015	−0.010 ± 0.058	−0.027 ± 0.034	−0.053 ± 0.014
56997	−0.033 ± 0.013	0.023 ± 0.025	−0.052 ± 0.025	−0.103 ± 0.048	−0.041 ± 0.026	0.042 ± 0.041
60314	−0.149 ± 0.023	−0.093 ± 0.040	−0.057 ± 0.018	−0.028 ± 0.033	−0.014 ± 0.028	−0.112 ± 0.058
62175	−0.111 ± 0.014	−0.108 ± 0.025	−0.032 ± 0.011	−0.013 ± 0.032	−0.014 ± 0.040	−0.054 ± 0.032
64150	0.024 ± 0.025	−0.151 ± 0.054	0.004 ± 0.025	0.008 ± 0.022	−0.005 ± 0.040	0.024 ± 0.013
64497	−0.118 ± 0.012	0.002 ± 0.025	−0.088 ± 0.025	−0.048 ± 0.050	−0.026 ± 0.032	−0.056 ± 0.057
64794	0.101 ± 0.023	0.097 ± 0.011	−0.042 ± 0.025	0.021 ± 0.020	0.019 ± 0.038	0.069 ± 0.025
72659	−0.008 ± 0.030	0.153 ± 0.031	−0.079 ± 0.025	−0.062 ± 0.028	−0.027 ± 0.024	0.086 ± 0.062
73815	−0.021 ± 0.045	0.020 ± 0.020	−0.028 ± 0.025	0.020 ± 0.023	0.013 ± 0.030	0.020 ± 0.041
74341	−0.059 ± 0.056	−0.054 ± 0.038	−0.024 ± 0.023	−0.049 ± 0.041	−0.029 ± 0.030	−0.018 ± 0.028
77466	0.250 ± 0.138	0.220 ± 0.030	0.016 ± 0.025	0.190 ± 0.055	0.095 ± 0.025	0.158 ± 0.100
78028	−0.013 ± 0.024	0.019 ± 0.038	−0.018 ± 0.025	−0.011 ± 0.039	0.022 ± 0.064	0.026 ± 0.017
78680	−0.089 ± 0.049	−0.035 ± 0.023	−0.115 ± 0.026	−0.116 ± 0.031	−0.057 ± 0.041	−0.075 ± 0.064
79186	0.154 ± 0.166	0.190 ± 0.040	−0.046 ± 0.025	0.108 ± 0.019	0.040 ± 0.032	−0.014 ± 0.024
79672	−0.113 ± 0.033	−0.041 ± 0.025	−0.042 ± 0.025	−0.038 ± 0.039	−0.010 ± 0.031	−0.047 ± 0.027
81512	−0.025 ± 0.023	−0.024 ± 0.018	−0.048 ± 0.025	0.018 ± 0.029	−0.026 ± 0.031	−0.048 ± 0.040
83601	−0.073 ± 0.068	−0.051 ± 0.030	−0.085 ± 0.014	−0.064 ± 0.018	−0.040 ± 0.037	−0.102 ± 0.113
88194	−0.050 ± 0.063	0.018 ± 0.011	−0.044 ± 0.025	0.023 ± 0.039	−0.003 ± 0.026	−0.060 ± 0.029
88427	0.125 ± 0.103	0.136 ± 0.024	0.005 ± 0.025	0.144 ± 0.036	0.045 ± 0.031	0.071 ± 0.019
89443	−0.068 ± 0.018	−0.059 ± 0.025	−0.040 ± 0.013	0.088 ± 0.019	0.004 ± 0.012	−0.072 ± 0.038
96895	0.007 ± 0.052	−0.002 ± 0.025	0.021 ± 0.025	0.068 ± 0.020	0.038 ± 0.046	−0.002 ± 0.040
96901	0.000 ± 0.075	0.005 ± 0.021	0.043 ± 0.037	0.072 ± 0.019	0.019 ± 0.064	0.010 ± 0.016
100963	−0.080 ± 0.028	−0.058 ± 0.043	−0.070 ± 0.025	−0.050 ± 0.055	−0.049 ± 0.036	−0.022 ± 0.028
102152	−0.004 ± 0.057	−0.021 ± 0.032	−0.034 ± 0.029	0.032 ± 0.016	0.016 ± 0.055	0.022 ± 0.034
104504	−0.070 ± 0.040	0.028 ± 0.041	−0.082 ± 0.023	−0.076 ± 0.033	−0.035 ± 0.031	−0.026 ± 0.058
107350	−0.086 ± 0.032	−0.060 ± 0.043	−0.091 ± 0.025	−0.042 ± 0.090	−0.027 ± 0.045	−0.125 ± 0.024
108708	−0.142 ± 0.030	−0.124 ± 0.049	−0.077 ± 0.025	−0.071 ± 0.020	−0.035 ± 0.049	−0.069 ± 0.051
108996	−0.063 ± 0.012	0.024 ± 0.035	−0.083 ± 0.035	−0.037 ± 0.050	−0.035 ± 0.043	−0.035 ± 0.073
109931	−0.015 ± 0.042	0.029 ± 0.033	0.039 ± 0.023	0.071 ± 0.016	0.057 ± 0.045	0.064 ± 0.044
113357	−0.057 ± 0.020	−0.093 ± 0.028	0.065 ± 0.025	0.040 ± 0.035	0.013 ± 0.030	0.008 ± 0.027
115604	0.012 ± 0.058	−0.043 ± 0.040	0.030 ± 0.030	0.041 ± 0.032	0.036 ± 0.041	−0.006 ± 0.016
118159	−0.091 ± 0.044	−0.045 ± 0.040	−0.158 ± 0.025	−0.104 ± 0.026	−0.062 ± 0.039	−0.061 ± 0.067

Table 3. Abundance ratios [X/Fe] for Ca, Sc, Ti, V, Cr, and Mn. Errors correspond to the 1-σ scatter of the line-by-line abundances. A conservative value of 0.050 for the error was assumed when only one line was available.

HIP	Ca	Sc	Ti	V	Cr	Mn
348	0.030 ± 0.070	0.036 ± 0.015	0.015 ± 0.041	0.028 ± 0.046	−0.011 ± 0.023	−0.074 ± 0.017
996	0.018 ± 0.037	0.057 ± 0.072	0.018 ± 0.025	0.023 ± 0.013	−0.009 ± 0.035	0.002 ± 0.026
1499	0.004 ± 0.033	−0.033 ± 0.025	−0.022 ± 0.025	−0.019 ± 0.020	−0.025 ± 0.041	0.062 ± 0.050
2131	0.059 ± 0.040	0.058 ± 0.056	0.064 ± 0.033	0.018 ± 0.041	−0.022 ± 0.032	−0.072 ± 0.018
2894	0.012 ± 0.020	0.080 ± 0.051	0.010 ± 0.029	0.002 ± 0.019	0.013 ± 0.036	−0.033 ± 0.025
4909	0.045 ± 0.052	0.074 ± 0.049	−0.028 ± 0.050	−0.009 ± 0.038	0.005 ± 0.035	−0.028 ± 0.024
5134	0.038 ± 0.029	0.014 ± 0.023	0.020 ± 0.051	−0.010 ± 0.039	−0.032 ± 0.027	−0.096 ± 0.031
6407	0.036 ± 0.019	0.024 ± 0.031	0.032 ± 0.036	0.046 ± 0.038	0.029 ± 0.021	−0.028 ± 0.025
7245	0.013 ± 0.045	0.026 ± 0.065	−0.001 ± 0.048	0.051 ± 0.040	−0.004 ± 0.039	0.030 ± 0.025
8507	0.048 ± 0.015	−0.000 ± 0.057	0.038 ± 0.038	0.002 ± 0.021	−0.002 ± 0.030	−0.075 ± 0.026
8841	0.023 ± 0.069	0.017 ± 0.057	0.016 ± 0.027	0.003 ± 0.033	−0.018 ± 0.033	−0.062 ± 0.037
9349	0.013 ± 0.038	0.025 ± 0.060	−0.002 ± 0.034	0.017 ± 0.013	−0.001 ± 0.050	−0.021 ± 0.018
10710	0.024 ± 0.039	0.013 ± 0.072	−0.027 ± 0.051	0.009 ± 0.043	0.005 ± 0.036	−0.046 ± 0.016
11728	0.042 ± 0.027	−0.025 ± 0.078	−0.014 ± 0.017	0.001 ± 0.030	−0.004 ± 0.036	0.005 ± 0.019
11915	0.021 ± 0.031	0.004 ± 0.041	−0.015 ± 0.029	0.006 ± 0.030	0.006 ± 0.019	−0.033 ± 0.018
14614	0.051 ± 0.039	0.025 ± 0.026	0.006 ± 0.034	−0.018 ± 0.019	−0.019 ± 0.027	−0.037 ± 0.032
14632	−0.003 ± 0.079	0.010 ± 0.033	−0.052 ± 0.054	−0.002 ± 0.038	−0.030 ± 0.021	−0.000 ± 0.025
18261	0.018 ± 0.028	−0.000 ± 0.057	0.002 ± 0.036	−0.028 ± 0.015	0.004 ± 0.034	−0.036 ± 0.019
22528	0.102 ± 0.045	0.097 ± 0.035	0.134 ± 0.065	0.066 ± 0.046	0.001 ± 0.042	−0.146 ± 0.025
23835	0.083 ± 0.028	0.111 ± 0.033	0.102 ± 0.029	0.052 ± 0.027	−0.007 ± 0.035	−0.132 ± 0.018
25670	0.035 ± 0.024	−0.037 ± 0.072	−0.011 ± 0.023	−0.019 ± 0.024	−0.008 ± 0.039	0.004 ± 0.013
28336	0.030 ± 0.061	0.017 ± 0.052	−0.001 ± 0.062	0.041 ± 0.040	−0.008 ± 0.013	−0.074 ± 0.017
38072	0.037 ± 0.091	0.025 ± 0.064	0.027 ± 0.029	0.023 ± 0.038	0.029 ± 0.027	−0.010 ± 0.025
38228	0.099 ± 0.063	0.036 ± 0.013	0.037 ± 0.054	0.035 ± 0.027	0.049 ± 0.051	−0.012 ± 0.023
42438	0.059 ± 0.041		0.026 ± 0.032	0.013 ± 0.083	0.068 ± 0.059	−0.081 ± 0.036
44324	−0.014 ± 0.028	0.010 ± 0.067	0.029 ± 0.080	0.023 ± 0.050	0.023 ± 0.063	−0.083 ± 0.019
46066	0.036 ± 0.027	0.042 ± 0.075	0.066 ± 0.021	0.033 ± 0.028	0.026 ± 0.040	0.000 ± 0.013
49572	0.023 ± 0.036	0.020 ± 0.107	0.015 ± 0.037	0.024 ± 0.034	−0.007 ± 0.050	−0.011 ± 0.028
49756	0.006 ± 0.061	0.043 ± 0.034	0.038 ± 0.014	0.047 ± 0.025	0.019 ± 0.046	0.003 ± 0.025
52040	0.054 ± 0.097	0.032 ± 0.034	0.043 ± 0.020	0.001 ± 0.033	0.028 ± 0.044	−0.046 ± 0.017
52137	0.018 ± 0.023	0.014 ± 0.063	0.042 ± 0.024	0.011 ± 0.025	0.032 ± 0.028	−0.029 ± 0.015
55459	0.009 ± 0.032	0.016 ± 0.032	0.028 ± 0.022	0.006 ± 0.017	0.017 ± 0.024	−0.029 ± 0.025
56948	−0.006 ± 0.034	0.013 ± 0.031	0.023 ± 0.028	−0.006 ± 0.031	0.034 ± 0.047	−0.005 ± 0.020
56997	0.017 ± 0.020	−0.025 ± 0.053	0.032 ± 0.014	0.020 ± 0.012	0.059 ± 0.028	−0.002 ± 0.025
60314	0.017 ± 0.036	−0.050 ± 0.050	0.070 ± 0.027	0.020 ± 0.021	0.022 ± 0.058	−0.013 ± 0.027
62175	0.018 ± 0.020	0.014 ± 0.020	0.042 ± 0.020	0.023 ± 0.025	0.030 ± 0.030	0.012 ± 0.027
64150	0.023 ± 0.035	−0.001 ± 0.044	0.013 ± 0.013	−0.011 ± 0.022	0.029 ± 0.034	−0.004 ± 0.022
64497	0.020 ± 0.033	0.024 ± 0.050	0.003 ± 0.035	0.004 ± 0.015	0.025 ± 0.031	0.002 ± 0.022
64794	0.015 ± 0.045	0.009 ± 0.058	0.023 ± 0.042	−0.031 ± 0.024	0.027 ± 0.050	−0.047 ± 0.013
72659	0.074 ± 0.029	−0.023 ± 0.046	0.042 ± 0.024	0.019 ± 0.019	0.047 ± 0.034	−0.036 ± 0.021
73815	0.008 ± 0.019	0.023 ± 0.018	0.036 ± 0.024	−0.005 ± 0.023	0.025 ± 0.034	−0.025 ± 0.019
74341	−0.004 ± 0.023	0.024 ± 0.072	0.027 ± 0.023	0.034 ± 0.019	0.041 ± 0.022	0.026 ± 0.028
77466	0.106 ± 0.037	0.074 ± 0.025	0.195 ± 0.019	0.110 ± 0.035	0.021 ± 0.045	−0.136 ± 0.023
78028	0.026 ± 0.069	0.020 ± 0.074	0.042 ± 0.045	0.031 ± 0.055	−0.013 ± 0.052	−0.015 ± 0.025
78680	0.007 ± 0.031	0.011 ± 0.012	−0.005 ± 0.036	−0.022 ± 0.035	0.007 ± 0.035	−0.054 ± 0.025
79186	0.071 ± 0.015	0.038 ± 0.078	0.100 ± 0.015	0.003 ± 0.033	−0.001 ± 0.025	−0.086 ± 0.034
79672	−0.003 ± 0.024	0.009 ± 0.015	0.031 ± 0.025	0.014 ± 0.012	0.030 ± 0.033	−0.009 ± 0.025
81512	0.016 ± 0.033	−0.008 ± 0.079	0.042 ± 0.014	−0.001 ± 0.024	0.022 ± 0.036	−0.054 ± 0.025
83601	0.039 ± 0.034	0.000 ± 0.022	−0.019 ± 0.039	−0.007 ± 0.053	−0.003 ± 0.023	−0.052 ± 0.040
88194	0.023 ± 0.023	0.006 ± 0.027	0.043 ± 0.014	−0.003 ± 0.027	0.010 ± 0.038	−0.042 ± 0.025
88427	0.065 ± 0.033	0.079 ± 0.019	0.135 ± 0.024	0.055 ± 0.027	−0.020 ± 0.025	−0.124 ± 0.017
89443	0.026 ± 0.033	0.036 ± 0.012	0.102 ± 0.021	0.057 ± 0.028	0.053 ± 0.060	−0.039 ± 0.013
96895	0.013 ± 0.036	0.030 ± 0.054	0.029 ± 0.027	0.042 ± 0.058	−0.003 ± 0.020	0.034 ± 0.016
96901	0.032 ± 0.045	0.002 ± 0.031	0.021 ± 0.028	0.010 ± 0.024	−0.000 ± 0.020	0.002 ± 0.022
100963	−0.009 ± 0.034	−0.002 ± 0.032	−0.021 ± 0.033	−0.018 ± 0.035	−0.013 ± 0.023	−0.038 ± 0.025
102152	0.014 ± 0.039	0.017 ± 0.027	0.029 ± 0.031	0.018 ± 0.023	0.010 ± 0.019	−0.025 ± 0.013
104504	0.035 ± 0.030		0.011 ± 0.052	0.006 ± 0.015	0.045 ± 0.040	−0.093 ± 0.015
107350	0.045 ± 0.056		−0.045 ± 0.021	0.002 ± 0.065	0.052 ± 0.091	−0.081 ± 0.028
108708	0.023 ± 0.031	−0.040 ± 0.079	0.006 ± 0.040	0.037 ± 0.024	0.026 ± 0.035	−0.007 ± 0.025
108996	0.046 ± 0.112	−0.007 ± 0.054	−0.024 ± 0.029	0.018 ± 0.016	0.032 ± 0.024	0.000 ± 0.010
109931	0.009 ± 0.015	−0.037 ± 0.106	0.026 ± 0.031	0.014 ± 0.021	0.017 ± 0.064	0.059 ± 0.030
113357	−0.015 ± 0.026	0.005 ± 0.031	−0.016 ± 0.022	0.009 ± 0.021	−0.011 ± 0.037	0.021 ± 0.013
115604	−0.006 ± 0.035	0.003 ± 0.039	0.036 ± 0.015	0.031 ± 0.015	0.016 ± 0.018	0.031 ± 0.039
118159	0.006 ± 0.033	0.070 ± 0.053	0.000 ± 0.055	0.015 ± 0.026	−0.007 ± 0.019	−0.073 ± 0.029

Table 4. Abundance ratios [X/Fe] for Ni, Cu, Zn, Y, Zr, and Ba. Errors correspond to the 1-σ scatter of the line-by-line abundances. A conservative value of 0.050 for the error was assumed when only one line was available.

HIP	Ni	Cu	Zn	Y	Ba	S
348	-0.001 ± 0.047	-0.003 ± 0.030	0.046 ± 0.050	-0.046 ± 0.041	-0.096 ± 0.050	-0.005 ± 0.014
996	0.019 ± 0.028	0.056 ± 0.062	0.116 ± 0.050	-0.039 ± 0.025	-0.046 ± 0.050	-0.013 ± 0.021
1499	0.057 ± 0.060	0.016 ± 0.069	0.027 ± 0.050	-0.034 ± 0.036	-0.086 ± 0.050	-0.013 ± 0.047
2131	-0.030 ± 0.023	-0.027 ± 0.025	0.095 ± 0.050	-0.121 ± 0.027	-0.130 ± 0.050	-0.025 ± 0.025
2894	-0.022 ± 0.036	-0.049 ± 0.054	-0.008 ± 0.050	0.078 ± 0.025	0.002 ± 0.050	0.136 ± 0.025
4909	-0.052 ± 0.039	-0.070 ± 0.046	-0.065 ± 0.050	0.055 ± 0.016	0.008 ± 0.050	0.204 ± 0.044
5134	-0.041 ± 0.033	-0.066 ± 0.013	-0.026 ± 0.050	0.061 ± 0.051	0.081 ± 0.050	0.134 ± 0.054
6407	-0.023 ± 0.039	-0.035 ± 0.081	-0.015 ± 0.050	0.045 ± 0.025	0.076 ± 0.050	0.143 ± 0.016
7245	-0.011 ± 0.043	-0.034 ± 0.022	0.027 ± 0.050	0.080 ± 0.025	0.065 ± 0.050	0.113 ± 0.057
8507	-0.034 ± 0.025	-0.073 ± 0.025	-0.046 ± 0.050	0.078 ± 0.021		0.110 ± 0.021
8841	-0.028 ± 0.030	-0.072 ± 0.011	0.072 ± 0.050	-0.071 ± 0.016	0.071 ± 0.050	0.004 ± 0.025
9349	-0.037 ± 0.029	-0.069 ± 0.030	-0.042 ± 0.050	0.078 ± 0.018	0.054 ± 0.050	0.151 ± 0.028
10710	-0.012 ± 0.053	-0.070 ± 0.016	0.006 ± 0.050	0.022 ± 0.042	0.037 ± 0.050	0.083 ± 0.025
11728	-0.012 ± 0.032	-0.035 ± 0.061	0.011 ± 0.050	-0.011 ± 0.025	0.005 ± 0.050	0.047 ± 0.018
11915	-0.026 ± 0.038	-0.064 ± 0.041	-0.071 ± 0.050	0.004 ± 0.025	0.130 ± 0.050	0.110 ± 0.011
14614	-0.022 ± 0.042	-0.050 ± 0.025	0.058 ± 0.050	0.009 ± 0.040	0.070 ± 0.050	0.084 ± 0.025
14632	0.030 ± 0.039	0.066 ± 0.025	0.042 ± 0.050	0.009 ± 0.025	-0.111 ± 0.050	0.003 ± 0.016
18261	-0.032 ± 0.022	-0.051 ± 0.057	0.057 ± 0.050	0.099 ± 0.022	0.064 ± 0.050	0.133 ± 0.011
22528	-0.018 ± 0.049	0.022 ± 0.045	0.215 ± 0.050	-0.095 ± 0.066	0.048 ± 0.050	-0.041 ± 0.025
23835	-0.013 ± 0.029	0.047 ± 0.054	0.088 ± 0.050	0.094 ± 0.036	0.123 ± 0.050	0.030 ± 0.035
25670	-0.016 ± 0.027	-0.047 ± 0.027	-0.007 ± 0.050	0.001 ± 0.011	0.016 ± 0.050	0.049 ± 0.018
28336	-0.024 ± 0.042	-0.065 ± 0.025	-0.091 ± 0.050	-0.008 ± 0.025	0.072 ± 0.050	0.072 ± 0.018
38072	-0.005 ± 0.032	-0.014 ± 0.079	-0.098 ± 0.050	0.036 ± 0.025	0.064 ± 0.050	0.114 ± 0.023
38228	-0.048 ± 0.099	0.709 ± 0.050	-0.147 ± 0.050	0.101 ± 0.045	0.018 ± 0.050	0.303 ± 0.025
42438	-0.093 ± 0.084	0.772 ± 0.050	-0.166 ± 0.050	0.039 ± 0.050	-0.049 ± 0.050	0.289 ± 0.045
44324	-0.027 ± 0.090	-0.115 ± 0.035	-0.026 ± 0.050	0.124 ± 0.052	0.030 ± 0.050	0.166 ± 0.050
46066	-0.045 ± 0.029	-0.042 ± 0.047	0.003 ± 0.050	0.070 ± 0.028	0.082 ± 0.050	0.117 ± 0.012
49572	-0.007 ± 0.033	-0.011 ± 0.057	0.065 ± 0.050	-0.058 ± 0.047	-0.005 ± 0.050	-0.012 ± 0.011
49756	-0.010 ± 0.050	-0.046 ± 0.025	-0.088 ± 0.050	0.064 ± 0.016	-0.020 ± 0.050	0.041 ± 0.035
52040	-0.030 ± 0.025	-0.065 ± 0.025	-0.001 ± 0.050	0.103 ± 0.064	0.025 ± 0.050	0.156 ± 0.025
52137	-0.049 ± 0.024	-0.109 ± 0.025	-0.105 ± 0.050	0.135 ± 0.025	0.087 ± 0.050	0.207 ± 0.011
55459	-0.008 ± 0.016	-0.024 ± 0.018	-0.019 ± 0.050	-0.000 ± 0.032	-0.031 ± 0.050	0.013 ± 0.025
56948	-0.006 ± 0.036	-0.032 ± 0.025	-0.015 ± 0.050	0.027 ± 0.016	0.110 ± 0.050	-0.010 ± 0.033
56997	-0.063 ± 0.017	-0.116 ± 0.023	-0.078 ± 0.050	0.094 ± 0.027	0.089 ± 0.050	0.174 ± 0.035
60314	-0.041 ± 0.054	-0.069 ± 0.016	-0.152 ± 0.050	0.093 ± 0.023	0.037 ± 0.050	0.039 ± 0.027
62175	-0.027 ± 0.020	-0.033 ± 0.011	-0.004 ± 0.050	0.080 ± 0.039	-0.002 ± 0.050	0.085 ± 0.052
64150	-0.019 ± 0.025	0.033 ± 0.016	-0.048 ± 0.050		0.148 ± 0.050	0.147 ± 0.025
64497	-0.057 ± 0.071	0.736 ± 0.050	-0.144 ± 0.050	0.060 ± 0.013		0.214 ± 0.063
64794	-0.028 ± 0.027	-0.019 ± 0.017	0.101 ± 0.050	-0.112 ± 0.025	0.016 ± 0.050	-0.051 ± 0.048
72659	-0.101 ± 0.035	-0.120 ± 0.059	-0.065 ± 0.050	0.091 ± 0.056	0.025 ± 0.050	0.301 ± 0.025
73815	-0.012 ± 0.022	0.001 ± 0.024	0.046 ± 0.050	-0.085 ± 0.023	-0.084 ± 0.050	-0.014 ± 0.035
74341	-0.014 ± 0.025	-0.043 ± 0.025	-0.123 ± 0.050	0.036 ± 0.031	0.076 ± 0.050	0.054 ± 0.025
77466	0.019 ± 0.042	0.042 ± 0.019	0.227 ± 0.050	-0.003 ± 0.024	-0.021 ± 0.050	-0.075 ± 0.014
78028	-0.000 ± 0.062	0.011 ± 0.045	-0.012 ± 0.050	0.096 ± 0.025	0.165 ± 0.050	0.019 ± 0.059
78680	-0.089 ± 0.040	0.647 ± 0.050	-0.039 ± 0.050	0.118 ± 0.011	0.141 ± 0.050	0.222 ± 0.015
79186	-0.034 ± 0.040	0.026 ± 0.025	0.103 ± 0.050	-0.039 ± 0.023	-0.144 ± 0.050	-0.027 ± 0.011
79672	-0.026 ± 0.011	-0.022 ± 0.049	0.012 ± 0.050	0.060 ± 0.022	0.121 ± 0.050	0.068 ± 0.025
81512	-0.008 ± 0.036	0.036 ± 0.028	0.058 ± 0.050	-0.025 ± 0.036	0.039 ± 0.050	0.032 ± 0.014
83601	-0.041 ± 0.063	0.731 ± 0.050	-0.164 ± 0.050	0.058 ± 0.025	0.010 ± 0.050	0.154 ± 0.058
88194	-0.022 ± 0.021	0.003 ± 0.011	-0.058 ± 0.050	-0.028 ± 0.018	-0.065 ± 0.050	0.024 ± 0.014
88427	0.013 ± 0.022	0.028 ± 0.014	0.141 ± 0.050	-0.044 ± 0.042	0.057 ± 0.050	-0.032 ± 0.033
89443	-0.017 ± 0.030	-0.004 ± 0.025	-0.020 ± 0.050	-0.017 ± 0.021	0.048 ± 0.050	-0.007 ± 0.013
96895	0.013 ± 0.018	0.058 ± 0.021	0.032 ± 0.050	-0.018 ± 0.011	-0.030 ± 0.050	-0.013 ± 0.025
96901	0.014 ± 0.021	0.037 ± 0.013	-0.004 ± 0.050	-0.058 ± 0.014	-0.019 ± 0.050	-0.041 ± 0.020
100963	-0.029 ± 0.028	-0.057 ± 0.025	-0.046 ± 0.050	0.100 ± 0.030	0.050 ± 0.050	0.108 ± 0.025
102152	-0.013 ± 0.027	0.018 ± 0.025	0.073 ± 0.050	-0.081 ± 0.025	-0.099 ± 0.050	-0.017 ± 0.025
104504	-0.066 ± 0.044	-0.094 ± 0.065	-0.019 ± 0.050	0.088 ± 0.012	0.051 ± 0.050	0.269 ± 0.025
107350	-0.090 ± 0.084		-0.142 ± 0.050	0.055 ± 0.050		0.221 ± 0.035
108708	-0.052 ± 0.029	-0.107 ± 0.040	-0.097 ± 0.050	0.025 ± 0.043	0.031 ± 0.050	0.175 ± 0.054
108996	-0.035 ± 0.053	-0.089 ± 0.035	-0.122 ± 0.050	0.064 ± 0.037	0.127 ± 0.050	0.150 ± 0.057
109931	0.026 ± 0.039	0.039 ± 0.025	0.033 ± 0.050	-0.065 ± 0.025	-0.093 ± 0.050	-0.035 ± 0.045
113357	0.021 ± 0.047	0.027 ± 0.055	0.004 ± 0.050	-0.027 ± 0.011	0.022 ± 0.050	-0.045 ± 0.025
115604	0.031 ± 0.024	0.057 ± 0.038	0.069 ± 0.050	-0.050 ± 0.033	-0.049 ± 0.050	-0.034 ± 0.011
118159	-0.052 ± 0.053	-0.124 ± 0.049	-0.131 ± 0.050	0.127 ± 0.025	0.137 ± 0.050	0.251 ± 0.014
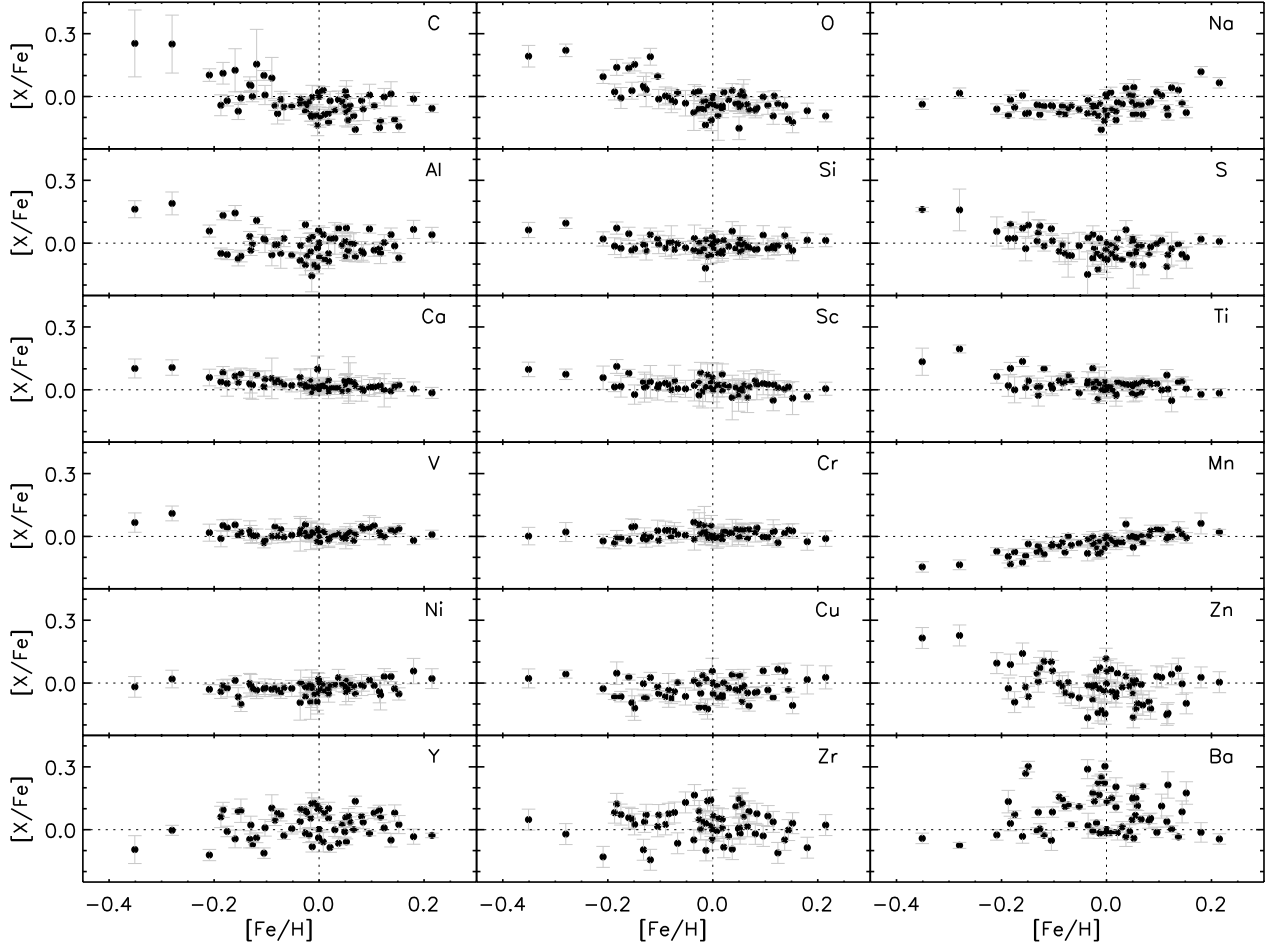
Fig. 1. Abundance ratios as a function of iron abundance for full sample of 64 stars. Dotted lines denote solar values.